



Expansion Wave Propagation into a Cavity

M. Whalley and B. Skews[†]

Flow Research Unit, School of Mechanical, Industrial and Aeronautical Engineering, University of the Witwatersrand, Johannesburg, 2050, South Africa

[†]*Corresponding Author Email: beric.skews@wits.ac.za*

(Received May 19, 2017; accepted October 5, 2017)

ABSTRACT

The flow field which results from an expansion wave entering a cavity from an upstream tube, and the focusing effect which occurs, is investigated. Different cavity geometries, different expansion wave pressure ratios and different expansion wave widths are explored. As the expansion wave propagates into the cavity it induces flow in the opposite direction and back down the walls. The flow experiences compression as it flows out back into the tube because of the concave surface of the cavity it encounters. This can result in the formation of shock waves which can propagate back up into the cavity. Very low pressure and temperature regions can develop because of the focusing action of the expansion. A convenient way of generating an expansion wave numerically and/or experimentally is in a shock tube. This consists of a tube divided into two compartments, one at high pressure and one at low pressure separated by a frangible diaphragm. On bursting the diaphragm, a shock wave travels in one direction and an expansion in the other towards the cavity. Whilst ideal boundary conditions can be imposed in numerical simulation laboratory experiments are complicated by the diaphragm being curved and having a finite opening time. The effect of an initially curved diaphragm is briefly considered. The expansion wave pressure ratio was altered by changing the initial pressure ratio across the diaphragm. For an initially high pressure ratio, supersonic flow can occur behind the trailing edge of the expansion wave which has a marked influence on the flow. The width of the wave is dependent on the distance of the diaphragm from the cavity and also has a significant influence on the flow. As the width of the wave increases and the density gradient decreases, focusing effects becomes significantly weaker. Correspondence between experiment and simulation is examined.

Keywords: Compressible flow, Unsteady flow, Wave focusing.

NOMENCLATURE

a	speed of sound	u	velocity
M	Mach number	γ	specific heat ratio
P	pressure	ρ	density
T	absolute temperature		

1. INTRODUCTION

Propagation of plane waves into a cavity have in the past been done using shock waves e.g. (Sturtevant and Kulkarny 1976; Izumi *et al.* 1994; MacLucas *et al.* 2015). Past studies of two-dimensional expansion wave interactions are very limited; one of the first is for diffraction on a corner (Mahomed and Skews 2014). Expansion waves are as common as compressions; an example is the fracture of a pressure vessel where a shock wave will propagate outward and an expansion wave inward. A good example is given in (Glass 1974) for the rupturing of a pressurized glass cylinder. Consider a plane-fronted expansion wave propagating into stationary gas in a tube. As it advances, the pressure will drop and will

cause the fluid to move in the opposite direction. If it were to strike an end wall, it will reflect and the pressure will drop still further. If the wall is not plane, a cavity flow results. A shock tube is an ideal facility for generating expansion waves. It consists of a straight tube separated into a high pressure section and a low pressure section with a frangible diaphragm between them. On bursting the diaphragm, a shock wave moves into the low pressure section and an expansion in the opposite direction. Figure 1 identifies four main regions on a distance/time wave diagram. The pressure ratio, $P_{41} = P_4 / P_1$, is the initial condition across the diaphragm, and $P_{43} = P_4 / P_3$ that across the expansion wave. The gas velocity and static pressure across the contact surface are identical i.e. $u_2 = u_3$

and $P_2 = P_3$. The relationship between the diaphragm pressure ratio and the shock pressure ratio, as given below, can be found in standard textbooks such as (Anderson 2003), based on the conservation equations of mass, momentum and energy. From this, and the conditions given above, the expansion wave pressure ratio P_{43} can be calculated, as well as the Mach number in region 3. These are shown in Fig. 1. The evaluation of the density and temperature behind the expansion wave can be determined from standard isentropic relations.

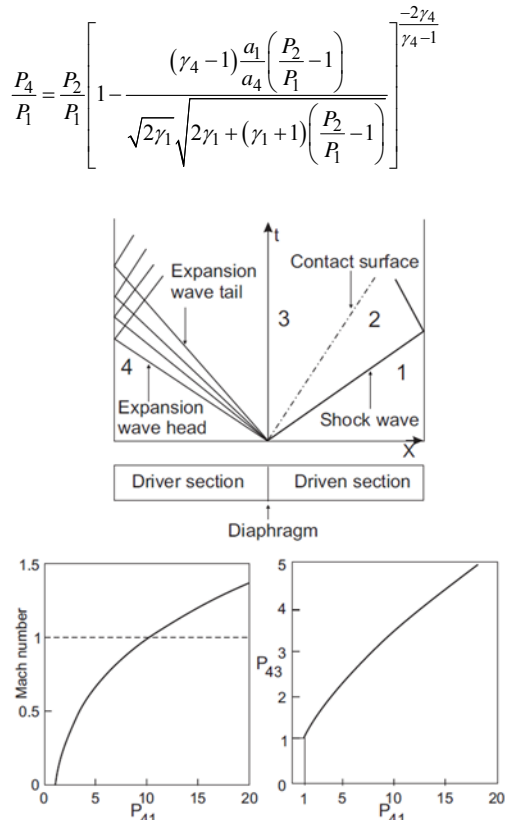


Fig. 1. Shock tube distance/time wave diagram (top). Mach number, M_3 , and expansion wave pressure ratio, P_{43} , as functions of diaphragm pressure ratio P_{41} .

Of particular note in the present study is that at a diaphragm pressure ratio of 10.4, for air, the Mach number in region 3 is sonic and the tail of the expansion will remain stationary at the diaphragm position. At higher ratios, the flow in region 3 becomes supersonic and the expansion tail will move down the tube in the same direction as the flow. As is evident, the expansion increases in width as it propagates, and thus the interrogation area needs to be positioned close to the diaphragm to keep the wave narrow, so that both the head and tail of the wave are within this area. Secondly, the density gradients become shallower in time, which makes flow visualisation very difficult, as will be discussed later.

2. NUMERICAL SIMULATION

The numerical simulations were done using the An-

sys Fluent 15.0 and STAR CCM+ 9 codes. The two-dimensional geometry was set up to coincide with a typical shock tube geometry, with a 100 mm square cross-section. The two regions of the tube were joined by an interface and all the external boundaries were set as walls as shown in Fig. 2. The low pressure region was made sufficiently long, 800 mm, so that reflected waves from the end do not interfere with the flow regions of interest. Three cavity shapes were considered: cylindrical, triangular and compound, as shown later.

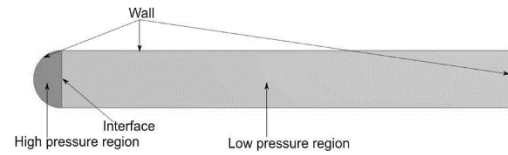


Fig. 2. Annotated geometry for numerical simulations.

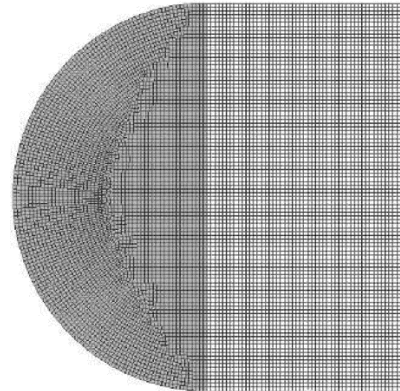


Fig. 3. Zoomed in view of interface for 1 mm base mesh.

The domain geometry was generated in Autodesk Inventor Professional 2016 and imported as a STEP file into ANSYS Workbench 16.2 DesignModeler, from which a two-dimensional surface was generated. The solver was set as density based planar. The solution method used is second order explicit upwind Roe-FDS type, with a Courant number of 0.5. In order to resolve the flow features particular to solutions involving shock waves and areas of large property gradients, adaptive mesh refinement macros were added. These involved adaption based on gradients of density with a normalised refinement threshold of 10%, every 100 iterations. Thus, cells in the domain with a gradient of above 10% of the maximum were considered for refinement. The maximum level of refinement was set at 3.

Simulations were run using base meshes with 2, 1, and 0.5 mm cell sizes, satisfying mesh independence. The flow features were consistent for all cases but since simulations did not take long to run the finer mesh, with refinement, was used. The area-weighted velocity and density at the wall was monitored for convergence and for comparing the different meshes. A typical mesh with 1 mm cell size is shown in Fig. 3. It is important to note to have the mesh aligned on either side of the inter-

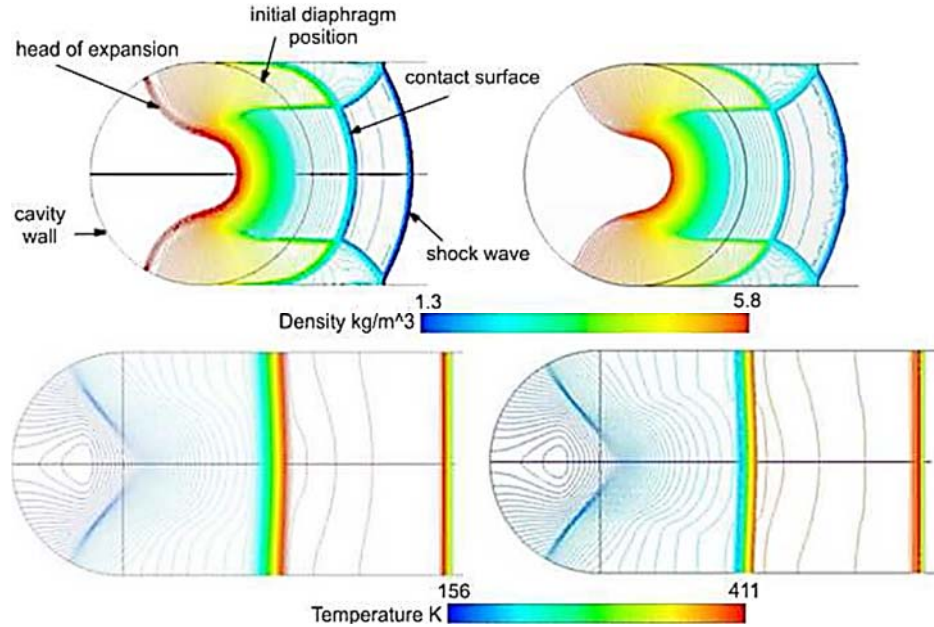


Fig. 4. Simulation results. Two images at the top show a comparison between the Fluent (left) and STAR solvers for a cylindrical diaphragm and a cylindrical cavity. The images below are for the fine mesh and a plane diaphragm, without and with adaption.

face in order to ensure the interface behaves correctly during the simulation.

Simulations were run using both of the codes, with the flow features being consistent as shown in the example in Fig. 4. The top row shows the result for a semi-circular diaphragm, such as occurs for a plastic diaphragm, with the head of the expansion entering a cylindrical cavity. The lower example shows a temperature plot resulting from a plane diaphragm with the shock and contact surface propagating into the driven section and oblique shocks developing in the cavity. Initial pressure and temperature in the low pressure driven tube were set at 101.3 kPa and 300 K.

3. RESULTS

A number of issues will be treated. Firstly, the main flow properties for the basic arrangements, followed by the influence of initial diaphragm curvature, and then that of the position of the diaphragm. The experimental results will then be treated.

3.1 Basic flow Features

The ideal case considered is where the initial expansion wave is plane, the diaphragm disappears instantaneously, and the test-piece is placed immediately adjacent to the diaphragm position. The three cavity profiles considered are cylindrical, triangular, and converging, the latter consisting of two quarter cylindrical surfaces placed symmetrically. Time-series plots for the three cavities are given in Fig. 5. In all cases a plane shock wave propagates to the right with the contact surface behind it, generated because of the different properties in regions 2 and 3 as shown in the wave diagram. The gas in region 2 is heated by passing

through the shock wave whereas that in region 3 is cooled from passage through the expansion wave. The shape of this surface is found to be dramatically influenced by the cavity shape. In the first frame, in all cases, the expansion wave has entered the cavity and reflect from its walls.

Consider the cylindrical cavity first. Since the testpiece is placed immediately adjacent to the diaphragm the expansion wave immediately enters the test piece at the top and bottom of the tube, and reflects towards the symmetry plane. The reflected expansion causes the fluid at the top and bottom of the tube to expand still further. The expansive flow causes the gas to move in the opposite direction down the wall towards the entrance of the cavity. Due to the concave curvature of the surface compression waves develop which then steepen up into shocks on both the upper and lower surfaces. (Generation of such shocks due to expansion wave propagation over both curved and plane surfaces is discussed in ([Skews and Paton 2016](#))). These shock waves meet on the symmetry plane and then reflect off each other in a regular reflection pattern. The two-dimensional expansion waves continue to reduce the pressure with the reflection point of the shocks arriving at the base of the cavity as shown in frame 4. This will be regarded as the end of focus. The lowest values of fluid properties occur just before this, as is shown later. The shock waves then reflect out of the cavity with changing complex profiles, through a transitioned regular reflection pattern, not shown, and then Mach reflection thereafter.

For the triangular cavity, the wall deflection angle is constant along the test-piece. The basic flow is similar to the cylindrical case, from the comparisons in Fig. 5, with the outward flow along

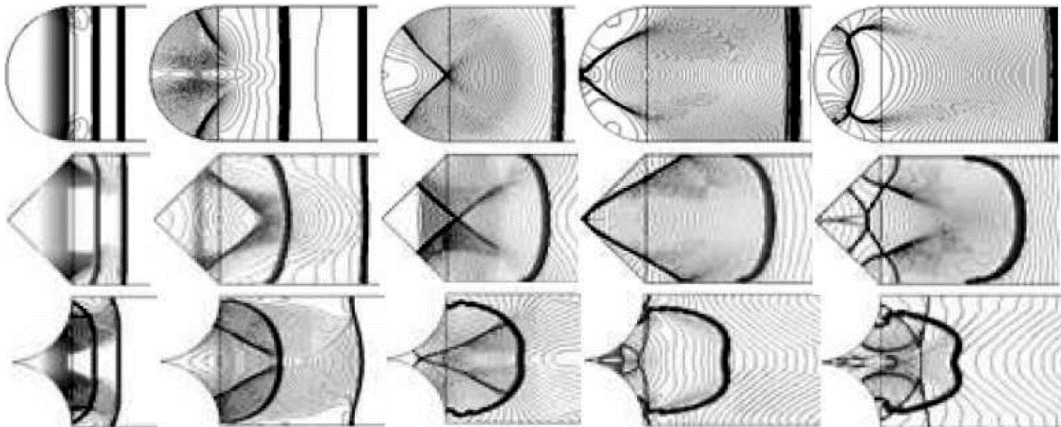


Fig. 5. Time series density contour plots for the three cavities, $P_{41} = 7$. 140 microseconds between images.

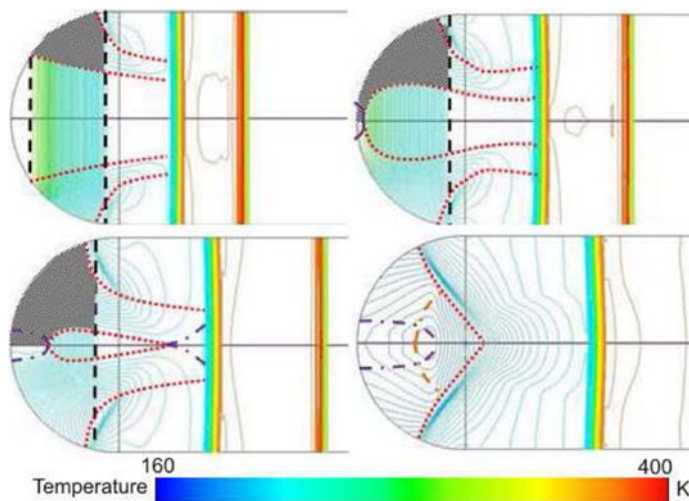


Fig. 6. Identification of wave propagation in the cylindrical cavity, , $P_{41} = 7$.

the surface resulting in a inward propagating shock wave due to it meeting the concave corner. These waves then meet at the cavity apex, (fourth frame), cross the symmetry plane, and reflect off the opposite surface. The reflected waves from either side then reflect off each other in Mach reflections with associated shear layers. An additional shock wave develops independently, normal to the surface. Its source will be treated later. A notable difference from the cylindrical case is that the effect the test-piece geometry has on the contact surface. The reflected expansion induces flow down the wall and away from the symmetry plane, resulting in a lower horizontal component of velocity compared to that on the symmetry plane. The resulting gas velocity profile affects the shape of the contact surface.

The third geometry, referred to as a converging cavity, consists of two quarter cylinders placed so that the cavity ends in a sharp point. The flow varies significantly from the previous two cases, as the reflected expansion affects both the contact surface and the initial shock from the diaphragm burst. The flow in the cavity itself is also different. The contact surface becomes almost stationary. On diaphragm

burst, the expansion wave immediately reflects off the front normal part of the cavity surface and thus interacts with the incident shock, causing it to curve by becoming locally weaker. Interior shock waves are also developed due to the flow down the surface of the cavity. Multiple reflections on the cavity surface and the symmetry plane then occur. This shock system moves out of the cavity with Mach reflections on either side, as shown in the last two frames, and will eventually become plane, and pass through the contact surface.

To more clearly show the propagation of the incident shock, contact surface and expansion wave, more detail is given in Figs. 6, 7 and 8. The leading and trailing edge of the initial expansion wave are shown by the dashed black lines. The red dotted lines represent the reflected expansion wave resulting when the incident expansion wave hits the walls of the cavity. The cross-hatched region is that which has been expanded by 2 expansion waves, both the initial expansion and the reflected expansion. Only the region above the symmetry plane has been highlighted in this way. In the remaining images, the cross-hatched region grows towards the symmetry plane.

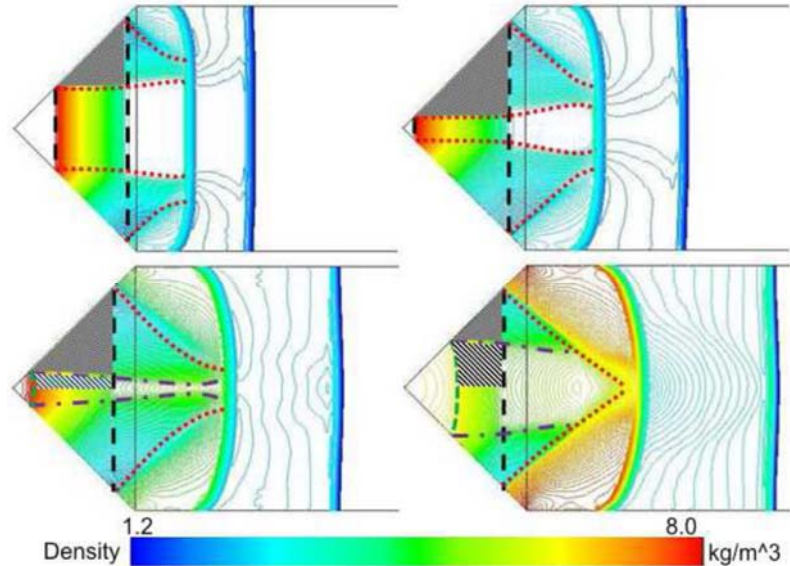


Fig. 7. Identification of wave propagation in the triangular cavity, , $P_{41} = 7$.

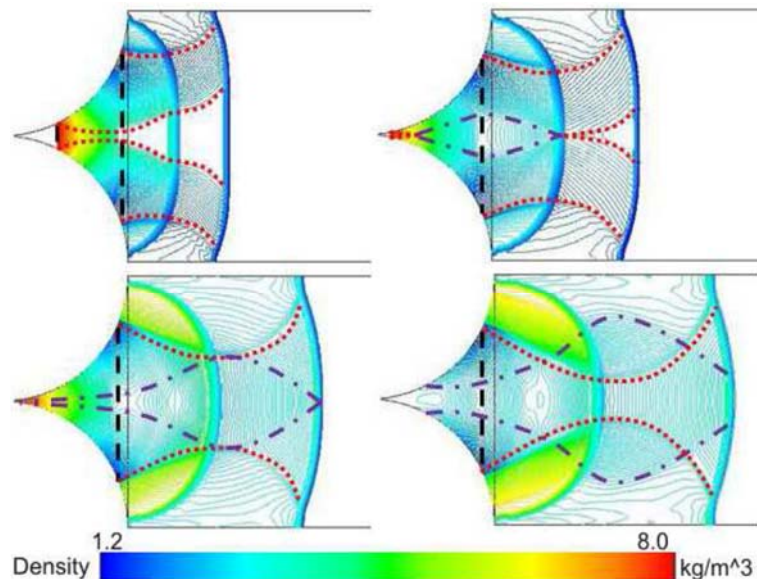


Fig. 8. Identification of wave propagation in the convex cavity, , $P_{41} = 7$.

When the leading edge of the reflected expansion wave has reached the symmetry plane, it reflects away from it; as shown by the purple dash-dot line. The expansion waves continue to reflect as the shocks converge, resulting in the region being expanded by multiple waves which causes a very low pressure region.

It is evident from the above that the flow field is complex. Additional insights are obtained from an examination of the flow directions. Figure 9 shows the vectors, coloured by velocity, with superimposed arrows to make it clearer, for the cylindrical cavity. The three images correspond to the wave patterns shown in the last three images for the cylindrical cavity in Fig. 5. In the top frame, slow outward flow occurs near the cavity surface, then accelerates towards the centre, becoming deflected inward by the oblique shocks, then

straightening out and accelerating to follow the contact surface. In the second frame, the flow directions within the cavity are reversed with flow towards the apex due to the reflection of the expansion wave. The same occurs for the one-dimensional reflection of an expansion wave from a plane surface. This leaves a temporary, almost stationary flow at the original diaphragm position. For the third frame, the wave system has developed into a pair of Mach reflections as shown in Fig. 5. The flow returns to be outward along the cavity walls becoming stationary at its base. The low velocity region moves out of the cavity with flow moving radially outward similar to what occurs for a source flow. The flow in the region of the triple points changes direction across all three shocks, that across the Mach stem also resulting in a temporary stagnant region.

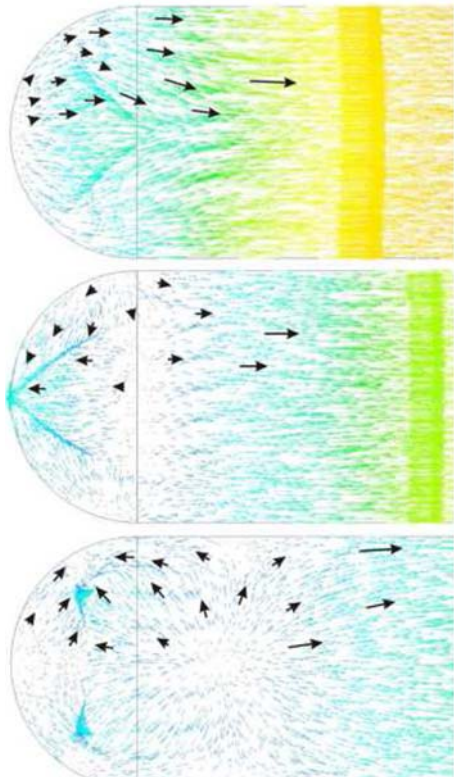


Fig. 9. Velocity vectors, coloured by velocity magnitude for the cylindrical cavity, , $P_{41} = 7$.

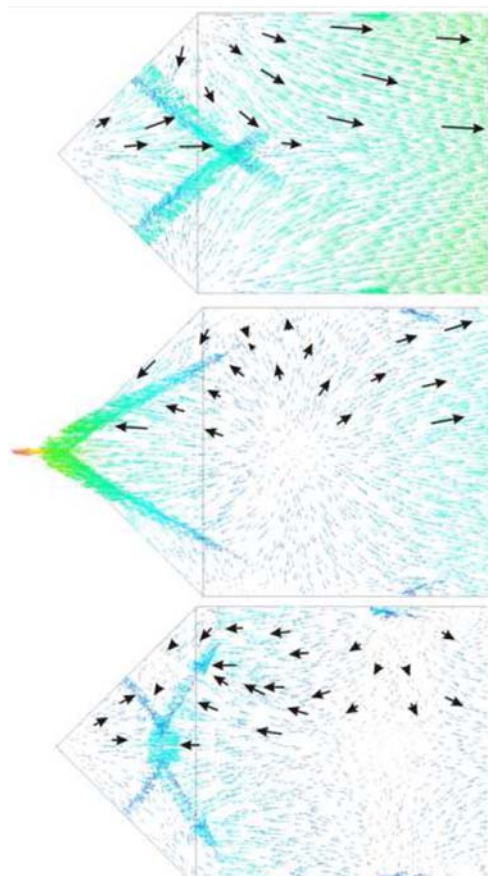


Fig. 10. Velocity vectors, coloured by velocity magnitude for the triangular cavity, , $P_{41} = 7$.

Figure 10 shows the vector plots for the triangular cavity, again corresponding approximately to the last three wave images given in Fig. 5. In contrast to the cylindrical case, for the oblique shock waves in similar positions as in the third frames in Fig. 5, the flow on either side of the shocks are in opposite directions due to stronger shock strengths. The flow also changes direction at the original diaphragm position. A high velocity is generated as the oblique shock waves converge on the apex and a very low velocity region with radial outflow also develops. As the shock wave system moves out of the cavity, a Mach reflection develops with gas flowing into the Mach stem from both directions at that particular instant. The shear layers emerging from the triple points, very evident in the density plot, indicate a slight change in flow direction on either side but is not directly evident in the vector plot. An interesting feature is that the density plot shows an additional shock wave (Fig. 5) separates from this Mach reflection pattern. This is an independent wave which is generated due to the approaching flow along the shock tube walls, moving into the cavity, encountering the concave corner and generating a shock wave terminating normal to the cavity surface. This wave is only vaguely evident in the vector plot due to flow on either side having similar direction. Also evident on the top and bottom walls is the termination of the highly curved contact surface which terminates on the wall at a shallow angle.

Three other simulations were run. One with a plane end wall (i.e. one-dimensional expansion wave reflection), and two for parabolic cavity profiles with aperture to depth ratios of 0.5 and 1.0, as shown in Fig. 11. The lowest pressure and temperature which occurs in the tube for the different geometries is given in Table 1. Comparisons of pressure history at the base of the three cavities for a lower diaphragm pressure ratio of $P_{41} = 3$ is given in Fig. 12. These values do not occur at the same time for the different geometries due to the differences in the flow, but they show for which geometry the focusing is the strongest, indicated by the lowest pressure and temperature as this implies the fluid has been expanded the most.

Table 1 Minimum pressure and temperature for different geometries, , $P_{41} = 7$, Initial pressure, $P_1 = 101.3 \text{ kPa}$, Initial temperature , $T_1 = 300 \text{ K}$.

Geometry	Minimum pressure [kPa]	Minimum temperature [K]
No test piece	72.7	157
Cylindrical	33.2	125
Triangular	6.8	80
Converging	1.4	50
Parabola AD 0.5	14.7	99
Parabola AD 1	16.9	103

3.2 Curved Diaphragm Effects

A perfectly plane diaphragm, at burst, cannot be

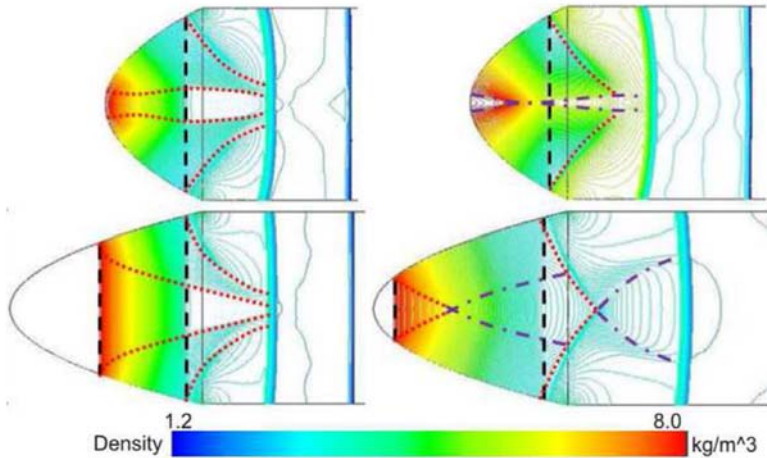


Fig. 11. Waves in parabolic cavities with depth to aperture ratios of 0.5 and 1.0., $P_{41} = 7.$, Contours of density.

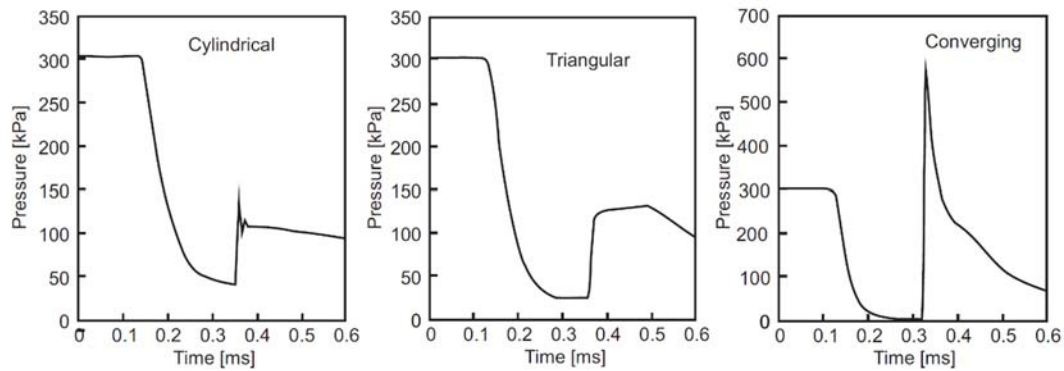


Fig. 12. Cavity base pressure traces from numerical simulation for the cylindrical, triangular and converging test pieces, , $P_{41} = 3.$

achieved experimentally due to the pressure difference across it so simulations were run with an initially curved diaphragm to see the effect this would have on the flow. The major concern with a curved diaphragm is the initial expansion wave will also be curved and thus there will be waves in the flow which are independent of the test-piece geometry used. The initial shock wave, propagating into the low pressure gas, will also be curved and will impact the upper and lower walls of the tube at an angle, from which it will reflect. An example of these reflected waves is given in Fig. 4 for a cylindrical test piece where the diaphragm is highly curved by 50% of the cavity height.

The expansion collapses towards the centre of the tube creating a region similar to the focus region seen in the ideal case, where a low pressure and temperature area is trapped between shock waves which gets smaller as the shock waves converge. Unlike the flow for the plane diaphragm case, this occurs independent of the cavity geometry. The expansion is still free to move into the cavity section. It is weaker and doesn't reflect off the test-piece geometry at an angle as large as in the plane diaphragm case. As a result, no shocks are formed in the cavity for this extreme case. The flow for the other cavity geometries is similar but shocks can occur for diaphragms with lesser curvature, as will

be shown below.

Wave diagram comparisons, along the symmetry plane, between a plane back wall and the cylindrical cavity for a plane and significantly curved diaphragm are shown in Fig. 13. The distance between the diaphragm clamping position and the base of the test piece was taken as 50 mm. The initial flow is almost identical for the two plane diaphragm cases but differs markedly for the curved diaphragm. This has maximum curvature 50 mm from the clamping position. The focusing then occurs outside the entrance to the cavity due to the converging expansion wave from the curved diaphragm.

3.3 Effect of Diaphragm Pressure Ratio.

Figure 14 shows the results for the cylindrical test piece at different diaphragm pressure ratios. For pressure ratios below 10.4, the fluid velocity downstream of the expansion wave is subsonic. This means that for these cases the trailing edge of the expansion wave moves into the cavity. For these pressure ratios the flow features are similar, with the strength of the waves increasing with increasing pressure ratio. At the diaphragm pressure ratio of 9 the flow starts to differ. This is due to the flow velocity downstream of the expansion wave being very close to sonic and thus the trailing edge of the

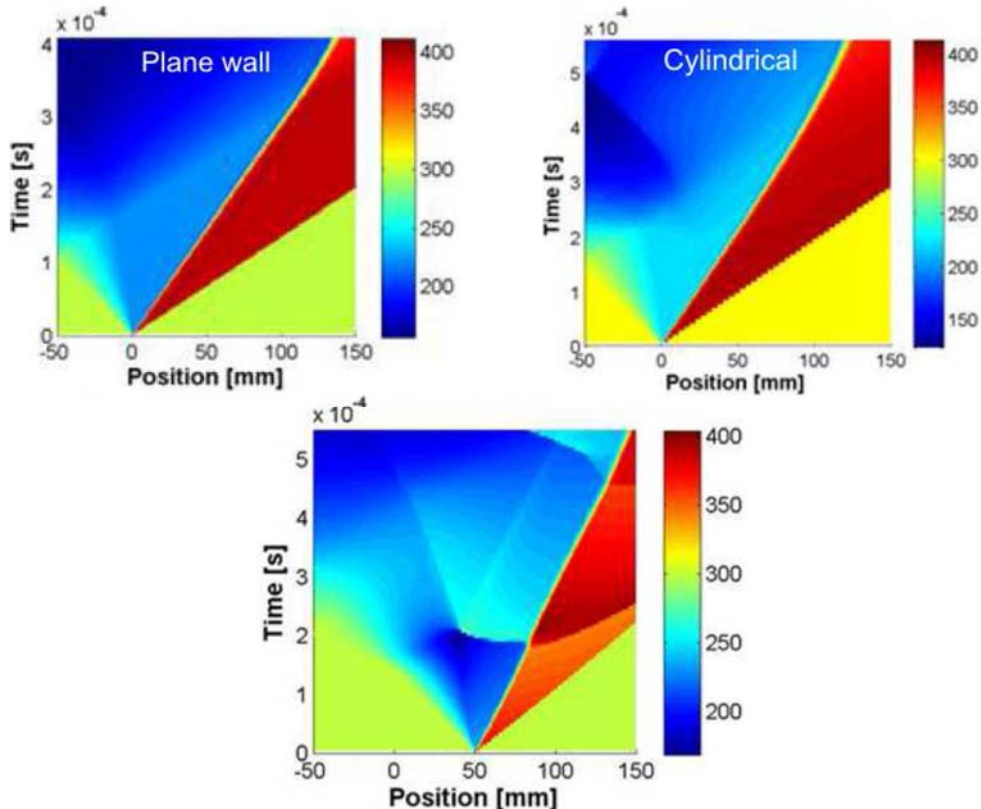


Fig. 13. Wave positions along the centre-lines vs time plots for a plane wall, and cylindrical cavities with the middle image for a plane diaphragm and the lower image with a 50% curvature, coloured by temperature.

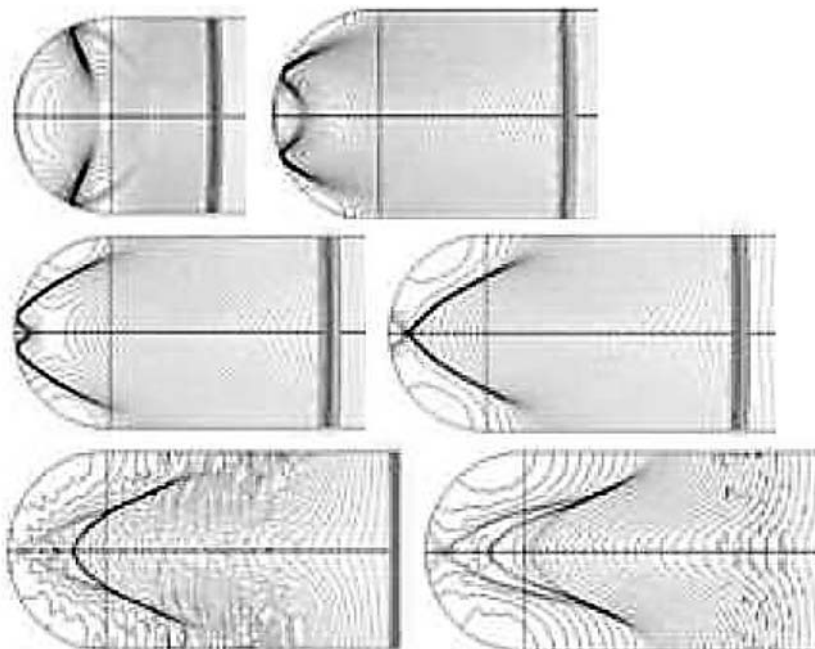


Fig. 14. Comparison of flow, at similar times, for diaphragm pressure ratios of 3, 5, 7, 9, 12, and 15.

expansion wave barely moves into the cavity. For diaphragm pressure ratios above 10.4, the flow is different. This is due to the flow velocity being supersonic with the trailing edge of the expansion wave traveling downstream. The main feature noted is that shocks do not form at the walls and move

into the cavity. Instead, shocks form at the cavity entrance and move transverse to the tube rather than along it. A similar series of simulations have been done for the triangular and converging cavities. The minimum temperature and pressure values are given in Fig. 15.

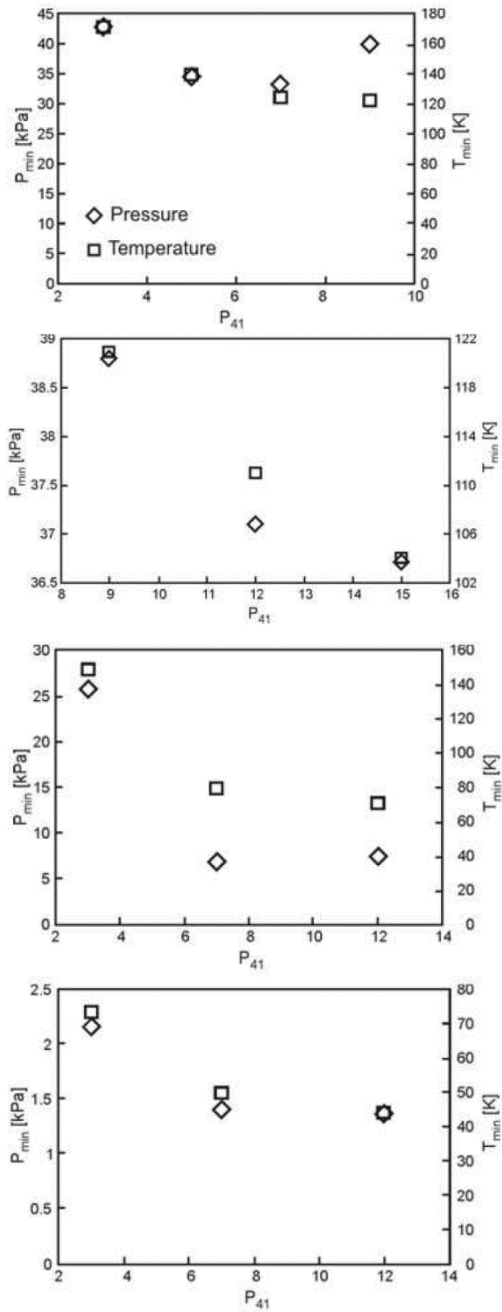


Fig. 15. Minimum pressures and temperatures for different pressure ratios. Upper two plots for the cylindrical cavity, and lower two plots respectively for the triangular and converging cavities.

3.4 Influence of Diaphragm Position

The distance of the test piece from the diaphragm is important because the density of the expansion wave flattens out as it travels away from the diaphragm, with significant reductions in the gradient. Figure 16 gives contour plots for the cylindrical test piece being placed 60 mm away from the diaphragm. Moving the test piece away from the diaphragm has a major effect on the focusing phenomenon. The focusing does not drop the flow properties sufficiently to cause strong compression waves to form and the transverse

waves are weak in relation to the main expansion wave. When the test piece is moved further away from the diaphragm the focusing becomes even weaker and the leading edge of the reflected expansion has become plane before it crosses the trailing edge of the initial expansion; this results in flow very similar to having a plane walled driver.

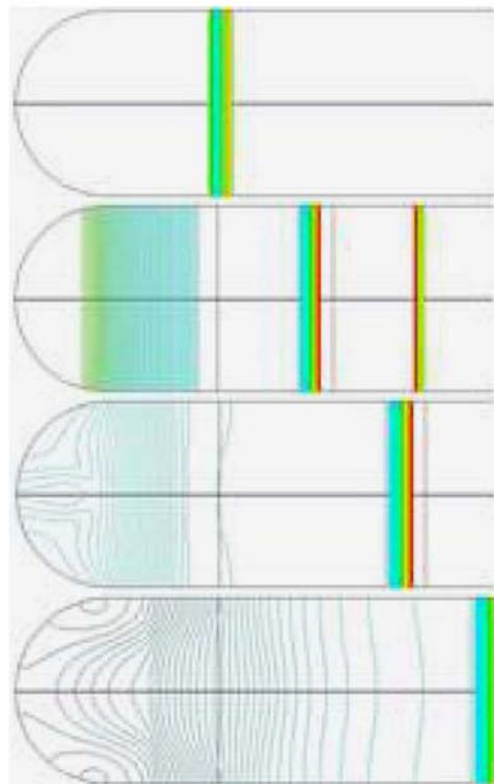


Fig. 16. Temperature contours for cylindrical test piece placed 60 mm from the diaphragm, , $P_{41} = 7$.

3.5 Comparison with Experiment

Experimentation on expansion waves using a shock tube are impacted by a number of issues. Firstly, the expansion increases in width as it propagates, as is evident from the wave diagram in Fig. 1, and thus the test section needs to be positioned close to the diaphragm to keep the wave narrow, so that both the head and tail of the wave are within the test section area. Secondly, the density gradients are weak, compared to shock waves, and become shallower in time, which makes visualisation rather difficult, also because of possible curvature of the diaphragm due to the pressure difference across it, as well as having a finite opening time. Idealized simulation studies were therefore done above with a plane diaphragm and instantaneous removal in order to establish basic flow properties, while briefly treating cases below to demonstrate some of the issues which depend on an experimental arrangement.

The shock tube employed was 100 mm high and 100 mm wide. The test pieces are manufactured from aluminium to form cylindrical, triangular and

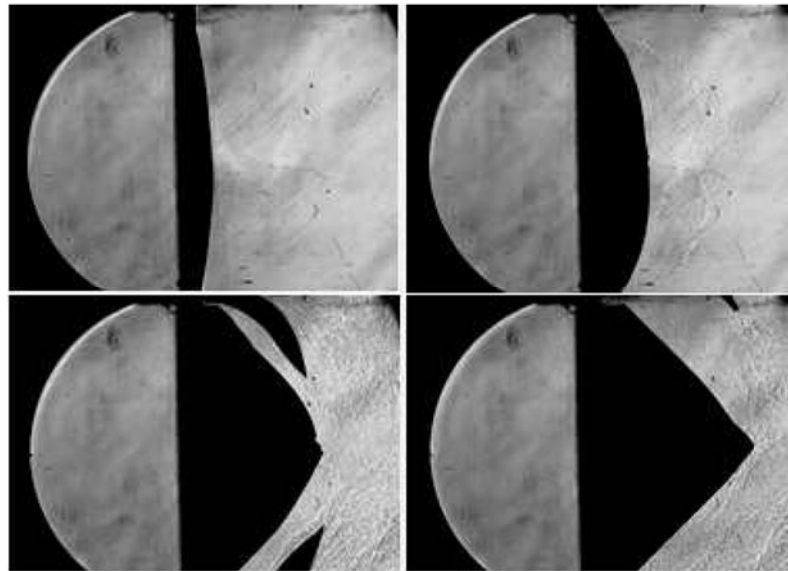


Fig. 17. Burst characteristics of Aluminium diaphragms. Time between frames: 150 μ s.

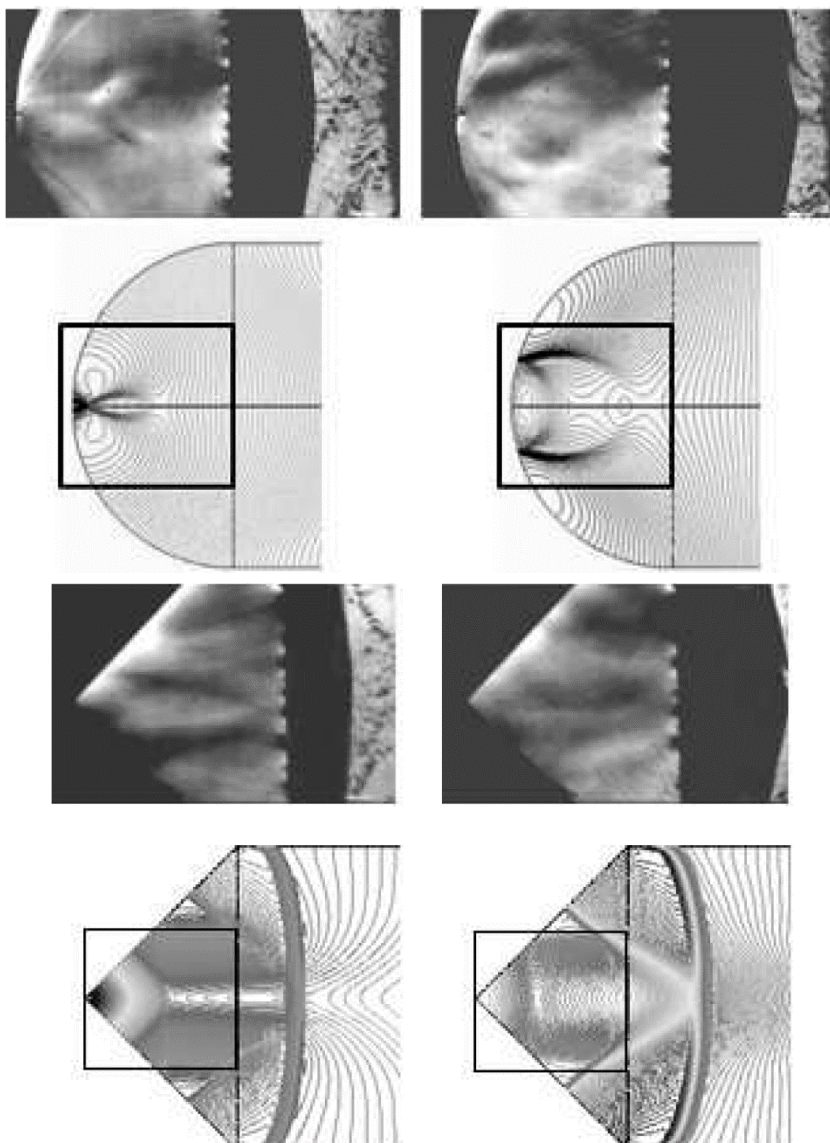


Fig. 18. Flow features seen in experimental images and corresponding numerical contour plots using a plane diaphragm., $P_{41} = 3$.

converging cavities of 50 mm depth. The tube design is rather unusual in that the diaphragm is clamped between two thin gaskets with windows on either side of it. This enables the diaphragm bursting process and the flow on either side to be examined in detail, which is important as the diaphragm separates two regions of different pressures and will deform before failure, resulting in a curved wave being initiated. A study into the burst characteristics of diaphragms made from several different materials was carried out. Three main criteria were used in the selection of the material: consistency, deflection, and burst pressure. The materials tested were: plastic, brass foil, copper foil, aluminium foil, and stainless steel foil. The plastic diaphragms, which are commonly used in shock tube studies deflected by an amount roughly equal to half the height of the test section and have been examined using numerical simulation as shown in Fig. 4 to show the effect, but were found to be unsuitable due to inconsistent rupture, besides causing wave focusing outside of the cavity and independent of it. Best results were found using 0.1 mm thick aluminium foil. Diagonal scoring resulted in consistent results with the triangular petals folding out as shown in Fig. 17. The first frame shows the deflection before failure. The second frame shows gas starting to escape with a fairly uniform front in the centre but inclined flow towards the top and bottom of the tube. The folding out of the petals is evident in the third frame and in the final frame the petals have folded out onto the tube and window surfaces leaving an unrestricted passage for the escaping gas. It is evident that the opening time is substantially larger than the time for the expansion to enter and interact within the cavity, as well as it not being planar.

Nevertheless, some results were obtained using a conventional z-configuration schlieren system and high-speed imaging, which show similar features to those of the simulation. Figure 18 shows a few results exhibiting some correspondence, at a diaphragm pressure ratio of 3, between a square section of the simulation shown as an outlined box, using a plane diaphragm, and experiment. It is interesting to note that even though the diaphragm is not fully open similar flow features are generated. It should be noted that schlieren with a horizontal knife-edge was used, therefore density gradients that appear dark in the upper half of the image will appear light in the lower half.

3.6 Conclusion

When an expansion wave enters a cavity it will create a reflection pattern which results in formation of regions of low pressure, temperature and density.

The shape of the focus region is affected by the initial shape of the expansion wave, with a curved expansion wave showing a weaker focus region than a plane wave entering a cavity. The greater the pressure drop over the initial expansion wave the stronger the focusing which occurs. The lower the gradient of the expansion wave, i.e. the further the expansion wave is from the initial diaphragm position in a shock tube, the weaker the focusing will be. Shock waves can form in the cavity region of a shock tube due to flow exiting the cavity meeting a concave surface or compression corner. Experimentation and visualisation is demanding and improved methods need to be explored. Three-dimensional effects due to curved diaphragm rupture and finite opening times significantly influence the flow patterns.

ACKNOWLEDGMENTS

The support of the South African National Research Foundation is gratefully acknowledged.

REFERENCES

- Anderson, J. (2003). Modern compressible flow with historical perspective. McGraw-Hill, New York.
- Glass, I. I. (1974). Shock Waves and Man. The University of Toronto Press.
- Izumi, K., S. Aso and M. Nishida (1994). Experimental and computational studies focusing processes of shock waves reflected from parabolic reflectors. *Shock Waves* 3, 213–222.
- MacLucas, D. A., B. W. Skews and H. Kleine (2015). High-speed imaging of shock wave cavity interactions using shearing interferometry and direction-indicating colour schlieren. *J. Visualization* 18, 521–529.
- Mahomed, I. and B. W. Skews (2014). Expansion wave diffraction over a 90 degree corner. *J. Fluid Mech.* 757, 649–664.
- Skews, B. W. and R. Paton (2016). Shock wave development within expansive flows. In K. Kontis (Ed.), *Proceedings of 22nd International Shock Interaction Symposium*, pp. 207–211.
- Sturtevant, B. and V. Kulkarny (1976). The focusing of weak shock waves. *J. Fluid Mech.* 76, 651–671.